Paper 256

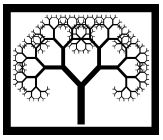

Proceedings of the Twelfth International Conference on
Civil, Structural and Environmental Engineering Computing,
B.H.V. Topping, L.F. Costa Neves and R.C. Barros, (Editors),
Civil-Comp Press, Stirlingshire, Scotland

Nonlinear Soil-Linear Structure Interaction: Energy and Strain Distribution

V. Gicev[1] and A. Hayir[2]
[1] Division of Computer Science
University "Goce Delcev", Macedonia
[2] Civil Engineering Faculty
Istanbul Technical University, Turkey

Abstract

The wave propagation approach in solving the problem is considered. The wave equation is solved numerically in the domain consisting of the soil, foundation, and superstructure using the explicit Lax-Wendroff numerical scheme. An artificial boundary is incorporated to simulate the Sommerfeld radiation boundary condition at infinity. The velocities and the displacements at the points of the stress-free boundaries are updated in each time step using the vacuum formalism approach.

The system consists of rectangular structure having circular foundation embedded in nonlinear soil. The aim of this study is to present the permanent strain distribution in a soil and to calculate energy distribution in a nonlinear system excited by SH waves in form of half-sine pulses. For that purpose, the superstructure and the foundation are assumed linear, while the soil as material is non-linear and is allowed to yield. Due to the plane waves, the input energy to the system, the hysteretic energy spent for creation and development of nonlinear strains, the scattered energy from the foundation, and the energy in the building are determined for half-sine pulses with same amplitude but different durations (frequencies). For transient response, we use dimensionless frequency, which is ratio between the radius of the semicircular foundation and half wavelength of the input pulse. The range of this dimensionless frequency in our analyses is from 0.05 (long pulses) to 2 (short pulses).

Keywords: nonlinear soil, permanent strain, energy distribution, SH waves, strong ground motion, Lax-Wendroff numerical scheme, flexible foundation.

1 Introduction

The effects of many earthquakes have provided numerous examples of different types of soil failure and permanent deformations caused by strong shaking. Many structures settle, tilt, or overturn on liquefied soil. Some of the best-known examples

of this occurred during the 1964 Alaska and 1964 Niigata earthquakes [1]. The sequence of the soil-structure interaction (SSI) phenomena, which led to the overturning of apartment buildings in Kawagishi-cho during the Niigata earthquake, is complicated, and its complete modelling and analysis are still a major challenge for any nonlinear numerical simulation. It probably started with development of nonlinear strain zones in the soil close to the foundation, which in turn expanded the trapped nonlinear energy to initiate liquefaction. We are assuming here that the large energy of earthquake waves trapped in the zones of strain localization initiated liquefaction [2], which then spread all around the foundation, causing the buildings to tilt and overturn. Analysis of this sequence is well beyond the scope of this paper, however. We will describe only the early stages, which involve the creation of the nonlinear zones of soil response.

The analytical solution for interaction of the wall sitting on an embedded semi-circular rigid foundation was presented in [3]. Wong and Trifunac [4] studied the wall-soil-wall interaction, while Abdel-Ghaffar and Trifunac [5] studied the soil-bridge interaction with a semi-cylindrical rigid foundation and an input plane-SH wave. Other studies have been conducted to analyze the influence of the shape of a rigid foundation on the interaction. Westermo and Wong [6] studied different boundary models for the soil-structure interaction of an embedded, semi-circular, rigid foundation. They concluded that without a transmitting boundary all of the models develop resonant behaviour and that the introduced damping in the soil cannot model the radiation damping. Luco and Wong [7] studied a rectangular foundation welded to an elastic half-space and excited by a horizontally propagating Rayleigh wave. V.W. Lee [8] solved a 3-D interaction problem consisting of a single mass supported by an embedded, hemispherical, rigid foundation for incident plane P, SV, and SH waves in spherical coordinates.

The recent publications deal with a flexible foundation. Todorovska et al. [9] solved an interaction of a dike on a flexible, embedded foundation, and Hayir et al. [10] described the same dike but in the absence of a foundation. Aviles et al. [11] analyzed the in-plane motion of a 4-degrees-of-freedom model and Gicev [12] studied the soil-flexible foundation-structure interaction for incident-plane SH waves with a numerical model using finite differences.

In this paper, in the presence of the interaction, the development of the nonlinear zones in the soil is studied for incident pulses representing the near-field destructive strong ground motion. The problems that must be addressed in the numerical study of the nonlinear soil-structure interaction include heterogeneities and discontinuities in the medium, the modelling of the free surface, artificial boundaries, and keeping track of the nonlinear constitutive law at each point in the soil. According to Moczo [13] and Zahradnik et al. [14], the computational FD schemes used in applications of wave propagation can be divided into homogenous and heterogeneous. Alterman and Karal [15] used the homogeneous formulation to solve elastic wave propagation in layered media, and Boore [16] proposed the heterogeneous scheme. Tsynkov [17] reviewed the existing global and local artificial boundaries.

2 Model

During the wave passage, the soil, the foundation, and the superstructure undergo nonlinear deformations and permanent strains. Because the aim of this paper is to study the nonlinear zones in the soil only, for simplicity, only the soil is modeled as nonlinear, while the foundation and the building are assumed to remain linear. The model is shown in figure 1.

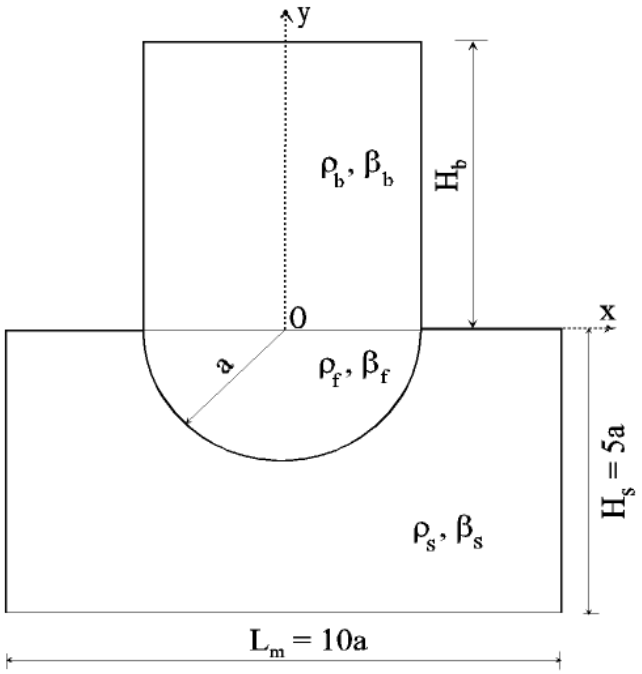

Figure 1: Soil-flexible foundation-structure system

The incoming wave is a half-sine pulse of a plane SH wave. A dimensionless frequency

$$\eta = \frac{2a}{\lambda} = \frac{a}{\beta_s \cdot t_{d0}} \tag{2.1a}$$

is introduced as a measure of the pulse duration, where a is the radius of the foundation, λ is the wavelength of the incident wave, β_s is the shear-wave velocity in the soil, and t_{d0} is duration of the pulse.

To set up the grid spacing, the pulse is analysed in space domain (s), and the displacement in the points occupied by the pulse is

$$w(s) = A \sin \frac{\pi \cdot s}{\beta_s \cdot t_{d0}}, \tag{2.1}$$

where A is the amplitude of the pulse and s is the distance of the considered point to the wave front in initial time in the direction of propagation. Using the fast Fourier transform algorithm, the half-sine pulse is transformed in wave number domain (k):

$w(k) = \mathfrak{F}(w(s))$. (2.2)

The maximum response occurs for k = 0 (rigid-body motion). As k increases, the response decreases and goes asymptotically to zero as k approaches infinity. We selected the largest wave number, $k = k_{max}$, for which the k-response is at least 0.03 of the maximum response (dashed lines in Figures 2a).

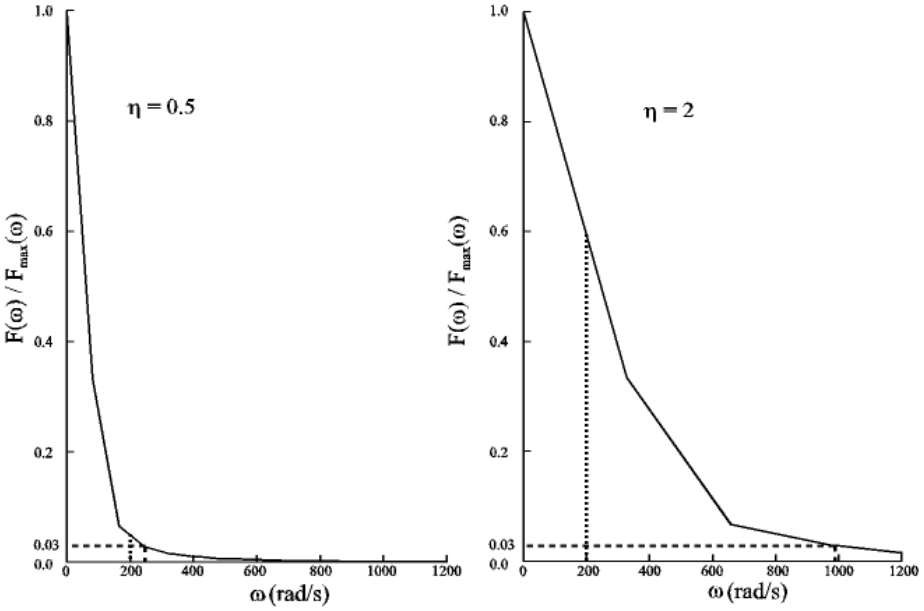

Figure 2a: Normalized one-sided frequency response:
a1) $\eta = 0.5$ a2) $\eta = 2$

Then, for this value of k_{max}, the corresponding frequencies and the corresponding wavelengths are computed:

$$\lambda_{min} = \frac{2\pi}{k_{max}} = \frac{2\pi\beta}{\omega_{max}}. \quad (2.3)$$

It can be seen from Fig. 2a that for $\eta = 0.5$, $\omega_{max} \approx 245\ rad/s$, while for $\eta = 2$, $\omega_{max} \approx 980\ rad/s$.

A measure of the numerical accuracy of the grid is related to the ratio between the numerical and physical velocity of propagation, $r = \frac{c}{\beta}$, which ideally should be 1. The parameters that influence this accuracy are:

- The density of the grid $m = \lambda / \Delta x$ (m is the number of points per wavelength λ, and Δx is the spacing between the grid points)
- The Courant number, $\chi = \beta_s \Delta t / \Delta x$
- The angle of the wave incidence, θ.

It has been shown in [18], [19], and [20] that the error increases when m decreases, χ decreases, and θ is close to 0 or $\pi/2$. For $O\left(\Delta t^2, \Delta x^2\right)$ approximation, the references above recommend m = 12.

To compare hysteretic energies and the nonlinear zones in the soil, the soil box should have the same dimensions for any dimensionless frequency of the pulse, η. For that reason, we chose a rectangular soil box with dimensions $\mathrm{L_m} = 10 \cdot \mathrm{a}$ and $\mathrm{H_s} = \dfrac{\mathrm{L_m}}{2} = 5 \cdot \mathrm{a}$ (Figure 1). Also, for merely practically reasons, the maximum number of space intervals in the grid in the horizontal (x) direction is set at 250 and in the vertical (y) direction at 400 (125 in the soil box and 275 in the building). The minimum spatial interval for a = 10m and for this setup is $\Delta \mathrm{x}_{\min} = \dfrac{\mathrm{L_m}}{250} = \dfrac{100}{250} = 0.4\,\mathrm{m}$. For a finer grid, the computational time increases rapidly. Having this limitation in mind, from Equation (2.3) and for $\eta = 2$ ($\omega_{\max} = 980\ rad/s$), the shortest wavelength is $\lambda_{\min} = 1.603\ m$, with the finest grid density $\mathrm{m} = \dfrac{\lambda_{\min}}{\Delta \mathrm{x}_{\min}} = \dfrac{1.603}{0.4} \approx 4\ points/\lambda_{\min} < \mathrm{m}_{\min}$.

Our numerical scheme is $O\left(\Delta t^2, \Delta x^2\right)$, so from the above recommendations we should have at least m = 12 points/$\lambda_{\min}$ to resolve for the shortest wavelength, $\lambda_{\min}$. This implies that the pulse should be low-pass filtered. A cut-off frequency $\omega_c = 200\ rad/s$ was chosen, and the pulse was low-pass filtered (Figure 2b). This implies that $\lambda_{\min} = 7.854\ m$ and then the grid density is

$$\mathrm{m} = \frac{\lambda_{\min}}{\Delta \mathrm{x}_{\min}} = \frac{7.854}{0.4} = 19.6\ points/\lambda_{\min} > \mathrm{m}_{\min}.$$

It can be seen from Fig. 2a (dotted lines) that for $\eta = 0.5$ only a negligible amount of the total power is filtered out, while for $\eta = 2$ a considerable amount is filtered out.

Also, it can be seen in Fig. 2b that for $\eta = 2$ the amplitude of the filtered pulse is smaller than the amplitude of the non-filtered pulse, which is A = 0.05 m, while for $\eta = 0.5$ the amplitude is almost equal with the amplitude of the non-filtered pulse.
From numerical tests, it has been shown that the viscous absorbing boundary rotated toward the centre of the foundation reflects only a negligible amount of energy back into the model [12]. For 2-D problems, the numerical scheme is stable if the time increment (Mitchell, 1969) is:

$$\Delta \mathrm{t} \le \min\left(\beta \sqrt{\frac{1}{\Delta \mathrm{x}^2} + \frac{1}{\Delta \mathrm{y}^2}}\right)^{-1}. \qquad (2.5)$$

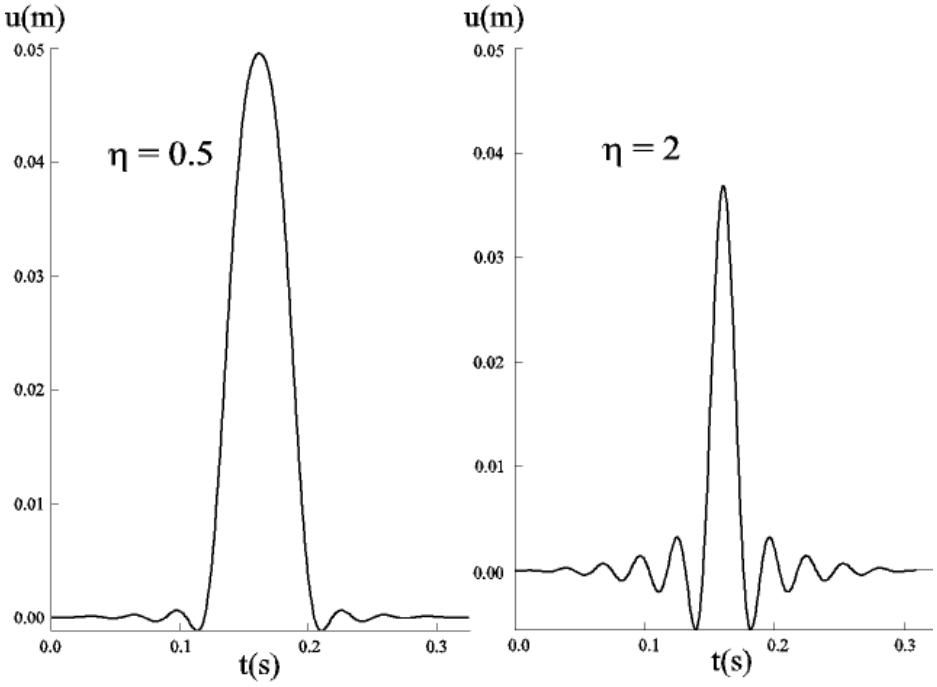

Figure 2b: Filtered pulse:
b1) $\eta = 0.5$, b2) $\eta = 2$

We assume that the shear stress in the x direction depends only upon the shear strain in the same direction and is independent of the shear strain in the y direction (and vice versa for shear stress in the y direction). The motivation for this assumption comes from our simplified representation of layered soil, which is created by deposition (floods and wind) into more or less horizontal layers. The soil is assumed to be ideally elastoplastic, and the constitutive $\sigma - \varepsilon$ diagram is shown in Figure 3. Further, it is assumed that the contacts remain bonded during the analysis and the contact cells C, D, E, F, G, and H in figure 4 remain linear, as does the zone next to the artificial boundary (the bottom four rows and the left-most and right-most four columns of points).

Neglecting the body forces in the z direction ($F_z = 0$), the wave equation is:

$$\rho \frac{\partial^2 w}{\partial t^2} = \left(\frac{\partial \tau_{xz}}{\partial x} + \frac{\partial \tau_{yz}}{\partial y} \right). \tag{2.6}$$

Introducing the new variables $v = \frac{\partial w}{\partial t}$, $\varepsilon_{xz} = \frac{\partial w}{\partial x}$, and $\varepsilon_{yz} = \frac{\partial w}{\partial y}$, and dividing (2.6) with ρ, the order (of 2.6) is reduced to the system of three first-order partial differential equations (PDE)

$$\underline{U}_{,t} = \underline{F}_{,x} + \underline{G}_{,y}, \tag{2.7}$$

where

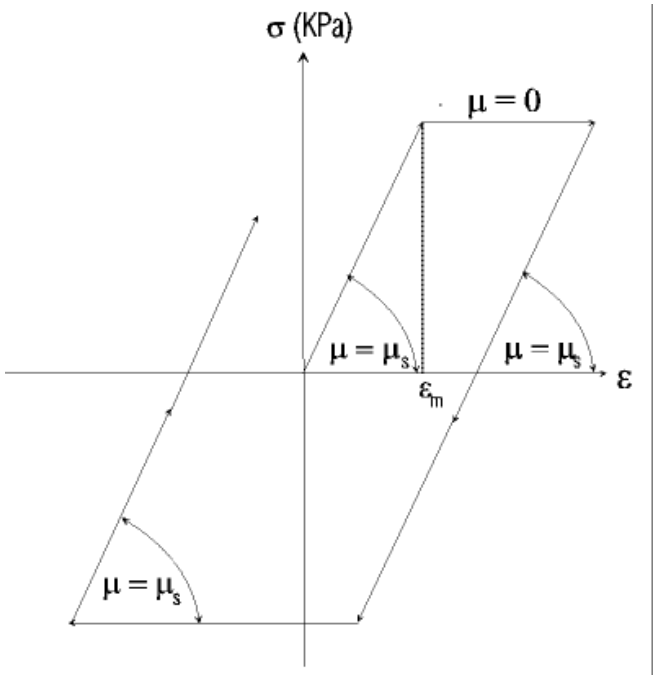

Figure 3: The constitutive law for the soil

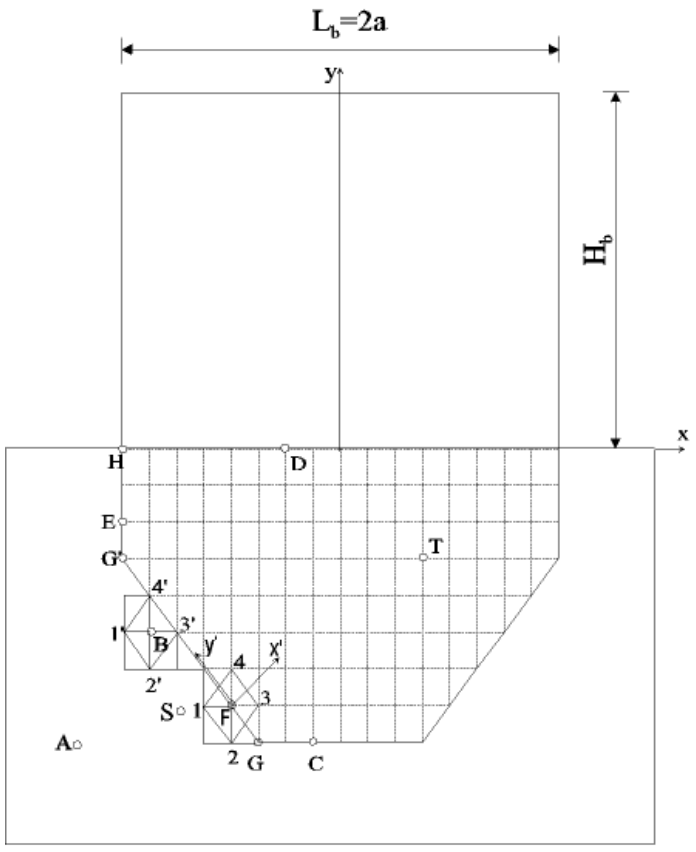

Figure 4: Numerical model with nonlinear soil. The points A, S, B, 1, 2, 1', and 2'can undergo permanent strains

$$\underline{U} = \begin{Bmatrix} v \\ \varepsilon_{xz} \\ \varepsilon_{yz} \end{Bmatrix} \qquad \underline{F} = \underline{F}(\underline{U}) = \begin{Bmatrix} \frac{1}{\rho}\tau_{xz} \\ v \\ 0 \end{Bmatrix} \qquad \underline{G} = \underline{G}(\underline{U}) = \begin{Bmatrix} \frac{1}{\rho}\tau_{yz} \\ 0 \\ v \end{Bmatrix}. \tag{2.8}$$

The first equation in (2.7) represents the dynamic equilibrium of forces in the z direction with neglected body force F_z, while the second and third equations give the relations between the strains and the velocity. The Lax-Wendroff computational scheme [22] is used for solving Equation (2.7) [12].

3 Energy and permanent strain distribution

As a test example, we consider a building with:
- height H = 18m,
- width L = 2a = 20m,
- shear wave velocities in the soil and in the building $\beta_s = \beta_b = 250\text{m/s}$,
- densities in the soil and in the building $\rho_s = 2500\text{kg/m}^3, \rho_b = 300\text{kg/m}^3$.

Majority of the buildings in Macedonia and Turkey have these properties.

A question arises about how to choose the yielding strain ε_m (figure 3) to study permanent strain distribution. The displacement, the velocity, and the linear strain in the soil during the passage of a plane wave in the form of a half-sine pulse are:

$$w = A\sin\left[\frac{\pi}{t_{d0}}\left(t - \frac{s}{\beta_s}\right)\right], \tag{3.1}$$

$$v = \dot{w} = \frac{\pi}{t_{d0}} A\cos\frac{\pi t}{t_{d0}}, \tag{3.2}$$

$$|\varepsilon| = \frac{v_{max}}{\beta_s} = \frac{\pi A}{\beta_s t_{d0}}. \tag{3.3}$$

Generally, the yielding strain can be written as

$$\varepsilon_m = C\frac{v_{max}}{\beta_s} = C\frac{\pi A}{\beta_s t_{d0}}, \tag{3.4}$$

where C is a constant that controls the yielding stress (strain) in the soil. We then consider the following cases of nonlinearity, depending upon C:

1. $C \geq 2$: **Small nonlinearity**. Permanent strain does not occur until the wave hits the foundation with any angle of incidence.
2. $1 \leq C < 2$: **Intermediate nonlinearity**. Permanent strain does not occur until the wave is reflected from the free surface or is scattered from the

foundation, for any angle of incidence. Permanent strain will or will not occur after the reflection of the incident wave from the free surface, depending upon the angle of incidence.

3. $C < 1$: **Large nonlinearity**. Permanent strain occurs after reflection from the free surface. Permanent strain may or may not occur before the wave reflects from the foundation surface, depending upon the angle of incidence.

3.1 Energy distribution in the system

The energy flow through a given area can be defined, in terms of a plane-wave approximation (Aki and Richards [23]), as:

$$E_{in}^{a} = \rho_s \cdot \beta_s \cdot A_{sn} \int_0^{t_{d0}} v^2 \cdot dt \quad , \tag{3.5}$$

where ρ_S and β_S are density and shear-wave velocity in the soil and v is a particle velocity (Equation (3.2)). A_{sn} is the normal area through which the wave is passing. For our geometrical setting (Figure 1), the area normal to the wave passage is:

$$A_{sn} = 2 \cdot H_s \cdot \sin\gamma + L_m \cdot \cos\gamma = L_m \cdot (\sin\gamma + \cos\gamma). \tag{3.6}$$

Inserting Eqs. (3.2) and (3.6) into (3.5) and integrating, the analytical solution for the input wave energy into the model is

$$E_{in}^{a} = \rho_s \cdot \beta_s \cdot L_m \cdot (\sin\gamma + \cos\gamma) \cdot \left(\frac{\pi \cdot A}{t_{d0}} \right)^2 \cdot \frac{t_{d0}}{2} \quad . \tag{3.7}$$

As can be seen from Equation (3.7), the input energy is reciprocal with the duration of the pulse and is a linear function of the dimensionless frequency η. Because the short pulses are low-pass filtered up to $\omega_c = 200\ rad/s$ (figure 2b), the analytical and the numerical solutions (3.5) for input wave energy do not coincide (figure 5).

Since our system is conservative, the input energy is balanced by:

- Cumulative energy going out from the model, E_{out}

$$E_{out} = \rho_s \cdot \beta_s \cdot A_{sn} \int_0^{T} v_R^2 \cdot dt \, , \tag{3.5a}$$

where v_R is the particle velocity from the outgoing field (scattered-from-foundation and radiated-from-building) while T is the time of the termination of the analysis.

- Cumulative hysteretic energy (energy spent for creation and development of permanent strains in the soil), computed from:

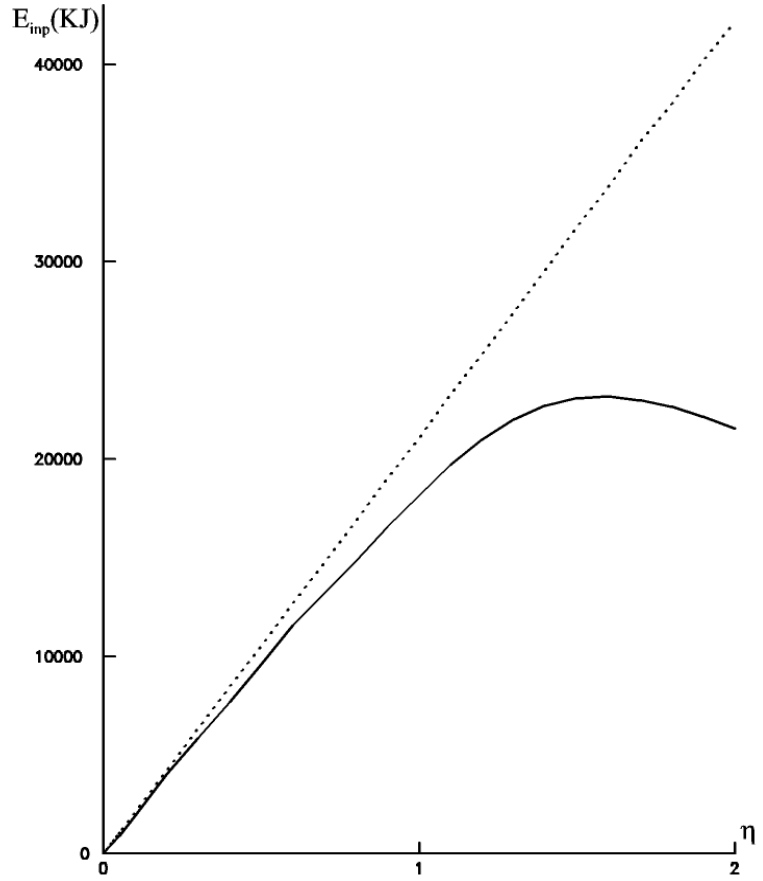

Figure 5 Input energy in the model vs dimensionless frequency:
- From analytic half-sine pulse (dashed line)
- From low-pass filtered half-sine pulse (solid line)

$$E_{hys} = \sum_{t=0}^{T_{end}} \Delta t \cdot \sum_{i=1}^{N} \left(\sigma_{xi} (\Delta \varepsilon_{xpi} + 0.5 \cdot \Delta \varepsilon_{xei}) + \sigma_{yi} (\Delta \varepsilon_{ypi} + 0.5 \cdot \Delta \varepsilon_{yei}) \right), \qquad (3.8)$$

where N is the total number of soil points; σ_{xi}, σ_{yi} are the stresses at the point i in the x and y directions respectively; $\Delta \varepsilon_{xpi} = \varepsilon_{xpi}^{t+\Delta t} - \varepsilon_{xpi}^{t}$ is the increment of the permanent strain in the x direction at point i; and $\Delta \varepsilon_{ypi} = \varepsilon_{ypi}^{t+\Delta t} - \varepsilon_{ypi}^{t}$ is the increment of the permanent strain in the y direction at point i.

- Instantaneous energy in the building, consisting of kinetic and potential energy, which can be computed from:

$$E_b = E_k + E_p = 0.5 \cdot \Delta x \cdot \Delta y_b \cdot \sum_{i=1}^{N} \left(\rho \cdot v_i^2 + \mu \cdot (\varepsilon_x^2 + \varepsilon_y^2) \right). \qquad (3.9)$$

In Fig. 6, this balance is shown for a pulse with $\eta = 1.5$, for incident angle $\gamma = 30^0$, foundation stiffness $\beta_f = 500 \text{m/s}$, and a yielding strain defined by C = 1.5 (Eq. 3.4).

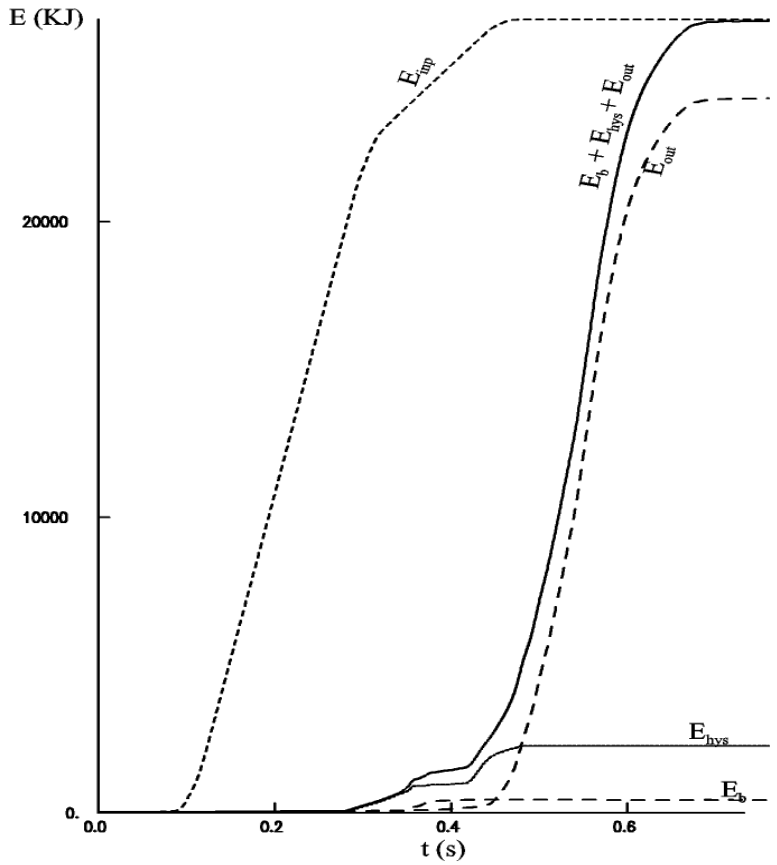

Figure 6 Energy balance in the model with foundation stiffness $\beta f = 500 m/s$ for $\gamma = 30$ and $\eta = 1.5$

To study the effect of scattering from the foundation only, the building is considered to be high enough so that the reflected wave from the top of the building cannot reach the building-foundation contact during the analysis. The analysis is terminated when the wave completely exits the soil island. In this study, the hysteretic energy in the soil and the energy in the building are the subjects of interest. In Figure 7, these two types of energy are presented as functions of the dimensionless frequency η.

Considering the energy entering the building (dashed lines), the results confirm the expectations that as the foundation becomes stiffer, a larger part of the input energy is scattered and less energy enters the building. In contrast, the results for hysteretic energy in the soil are not so straightforward. For an angle of incidence $\gamma = 60^0$, the hysteretic energy of the model with the softest considered foundation reaches the maximum value $E = 2674KJ$ at $\eta = 1.4$. This is the maximum hysteretic energy for all considered cases, while for an angle of incidence $\gamma = 30^0$, the hysteretic energy of the model with $\beta_f = 500 m/s$ is the largest with maximum value $E = 2265KJ$ at $\eta = 1.4$.

The reason for these irregularities is constructive and destructive interference among the incoming, reflected and scattered waves from foundations with different stiffness.

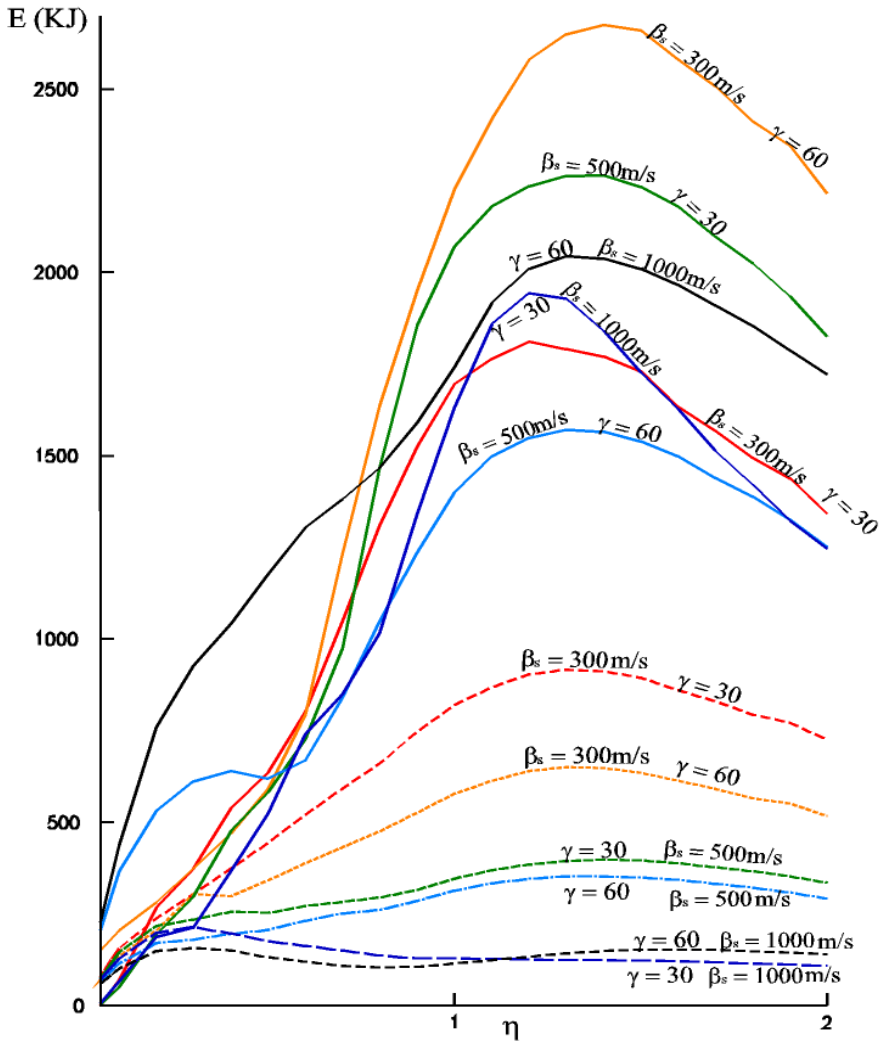

Figure 7 Hysteretic energy (solid lines) and energy entering the building (dashed lines) vs. dimensionless frequency for intermediate nonlinearity C = 1.5

3.2 Distribution of the permanent strain in the soil

Considering Figure 8, and starting from dynamic equilibrium of the differential body, we can find the principal stress at a point and its direction as:

$$\tau_{zp} = \tau_{zx}\cos\gamma + \tau_{zy}\sin\gamma$$

$$\gamma = \tan^{-1}\frac{\tau_{zy}}{\tau_{zx}}.$$

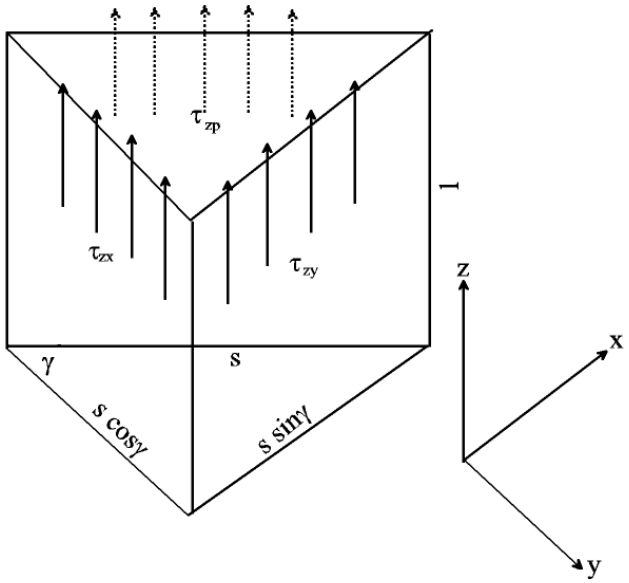

Figure 8 Orthogonal and principal shear stresses on differencial pentahedron

In Figures 9 a, b, c, d the principal permanent strain in the soil is illustrated for the case of small nonlinearity (C = $\sqrt{3}$) for two angles of incidence, $\theta = 30^0$ and 60^0, and for three foundation stiffness, β_f = 300 m/s; 500 m/s; and 1000 m/s. This value of C guarantees that for angles of incidence $30^0 \le \gamma \le 60^0$ there is no occurrence of permanent strain until the wave hits the foundation.

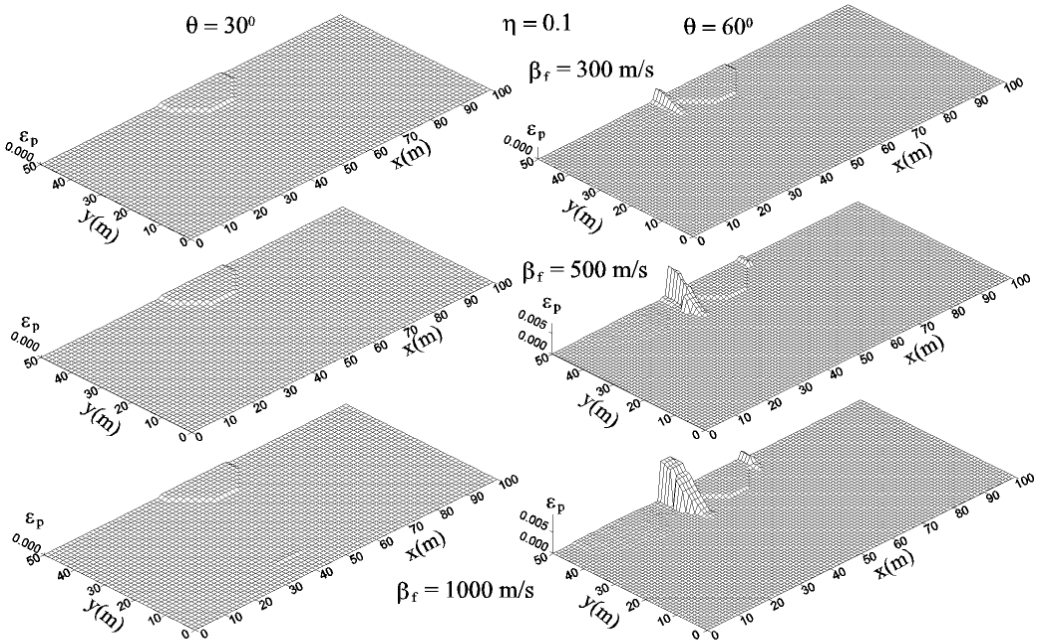

Figure 9a Principal permanent strain in the soil for η = 0.1, two angles of incidence, and three foundation stiffness. C = 1.73

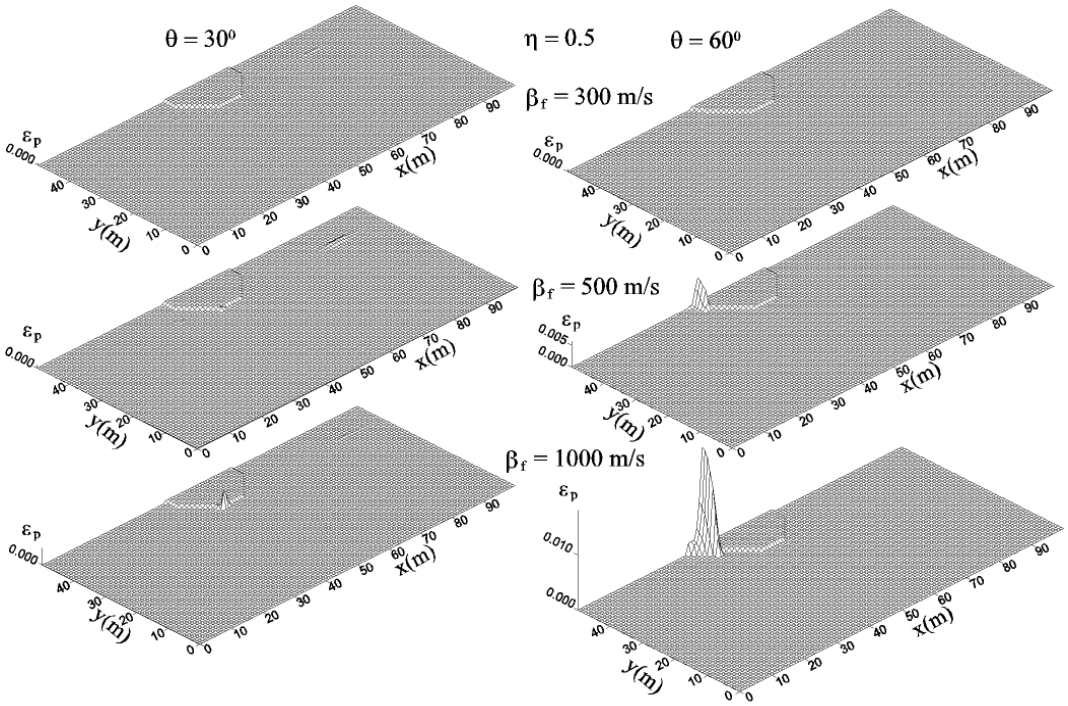

Figure 9b Principal permanent strain in the soil for $\eta = 0.5$, two angles of incidence, and three foundation stiffness. C = 1.73

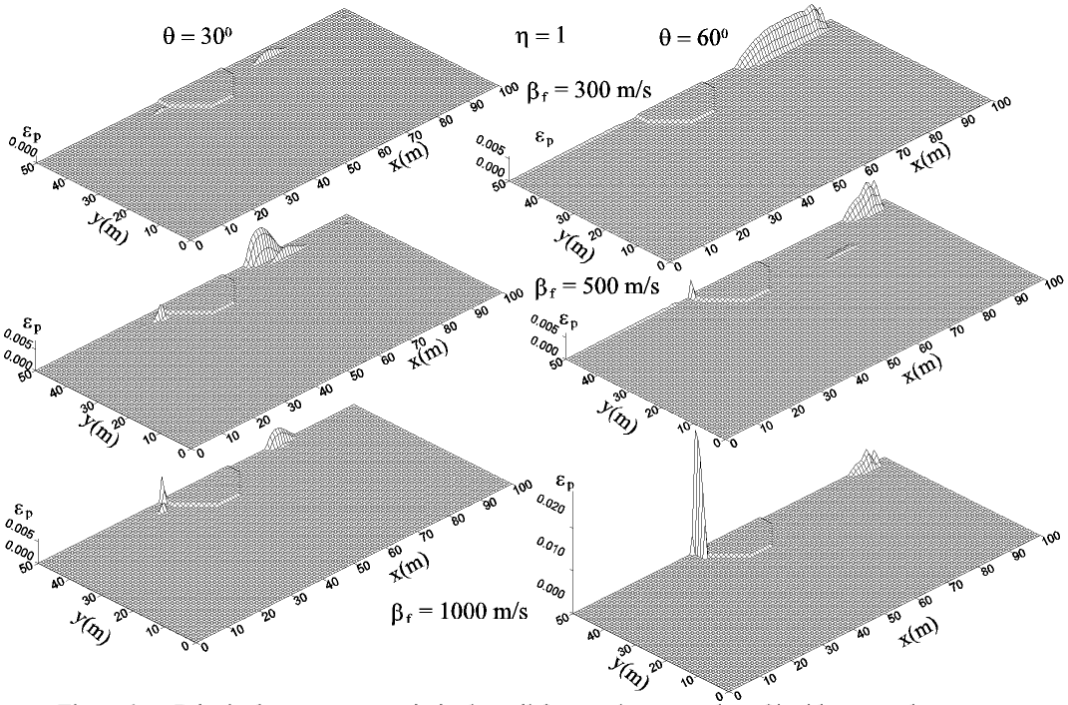

Figure 9c Principal permanent strain in the soil for $\eta = 1$, two angles of incidence, and three foundation stiffness. C = 1.73

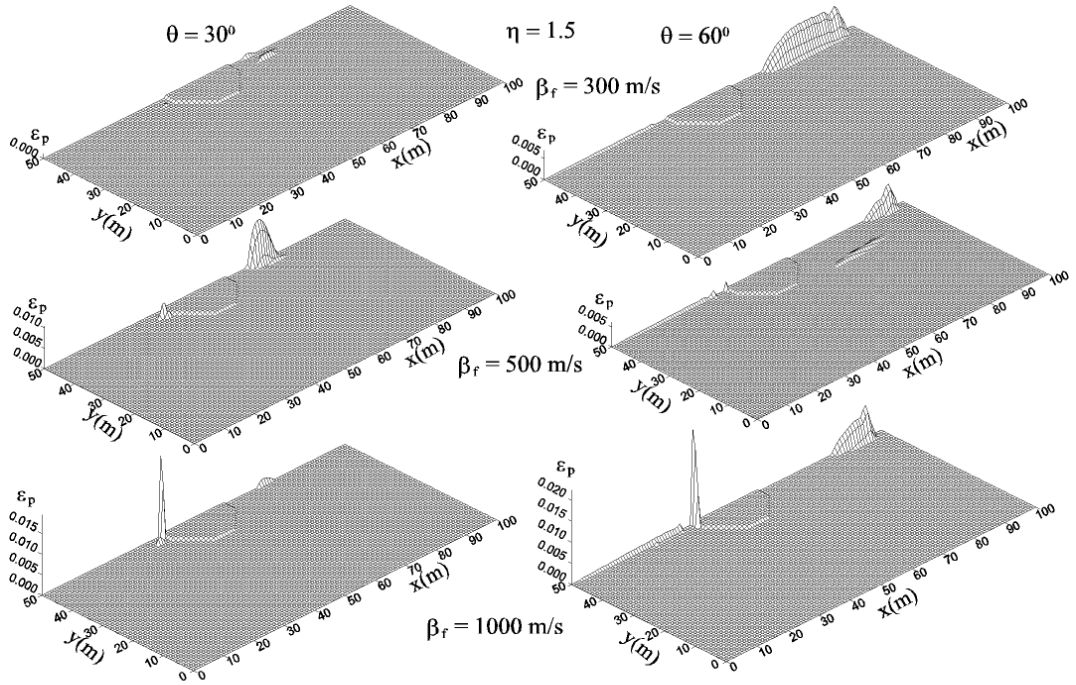

Figure 9d Principal permanent strain in the soil for η = 1.5, two angles of incidence, and three foundation stiffness. C = 1.73

Figures 10 a, b, c, d are the same as figures 9 a, b, c, d, but for the case of intermediate nonlinearity (C = 1.5).
In this case, permanent strain occurs before the wave hits the foundation, but after it reflects from the free surface.

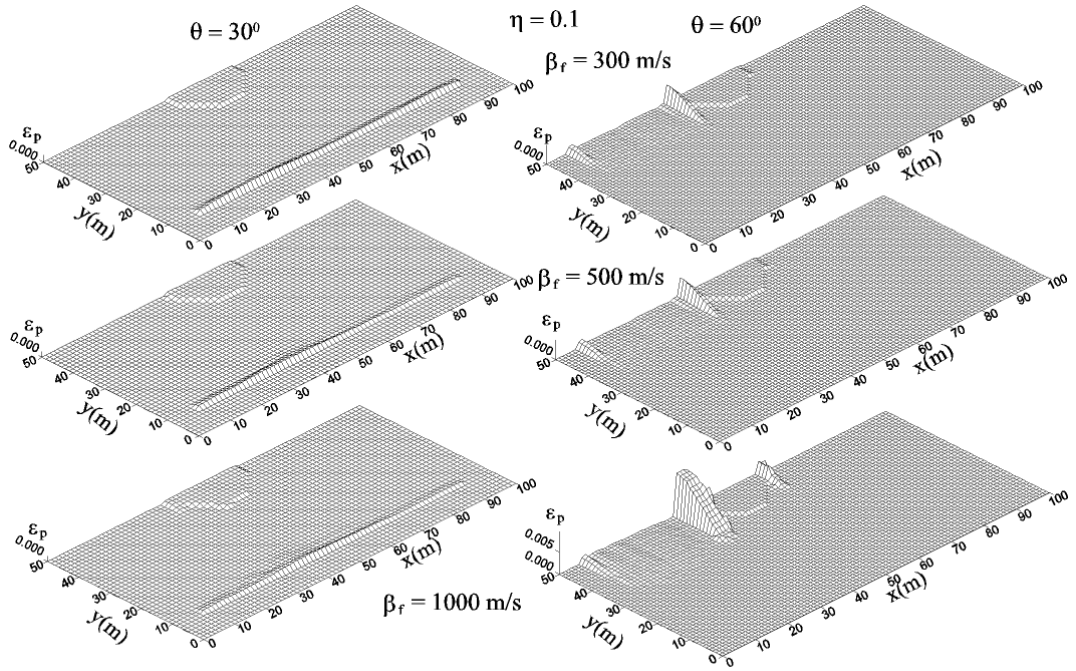

Figure 10a Principal permanent strain in the soil for η = 0.1, two angles of incidence, and three foundation stiffness. C = 1.5

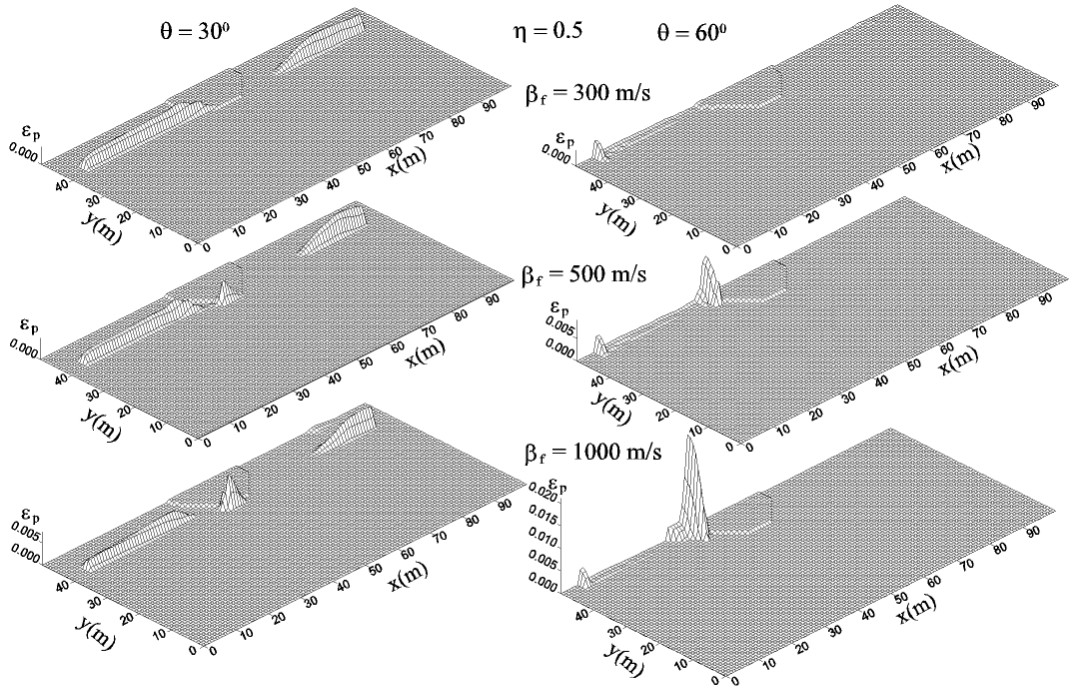

Figure 10b Principal permanent strain in the soil for η = 0.5, two angles of incidence, and three foundation stiffness. C = 1.5

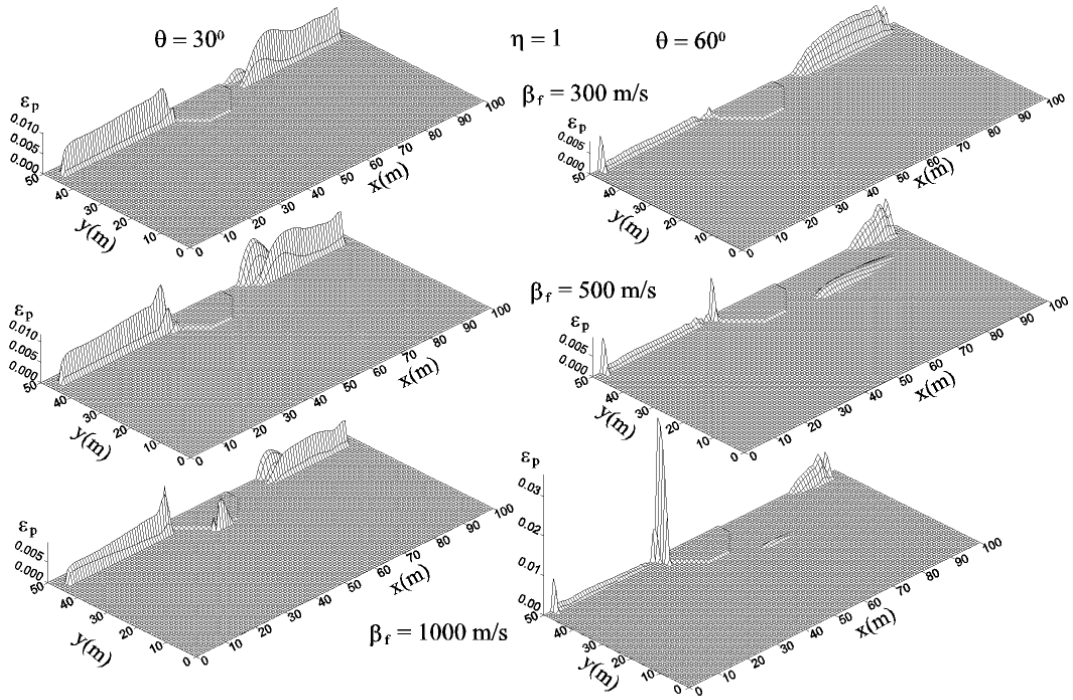

Figure 10c Principal permanent strain in the soil for η = 1, two angles of incidence, and three foundation stiffness. C = 1.5

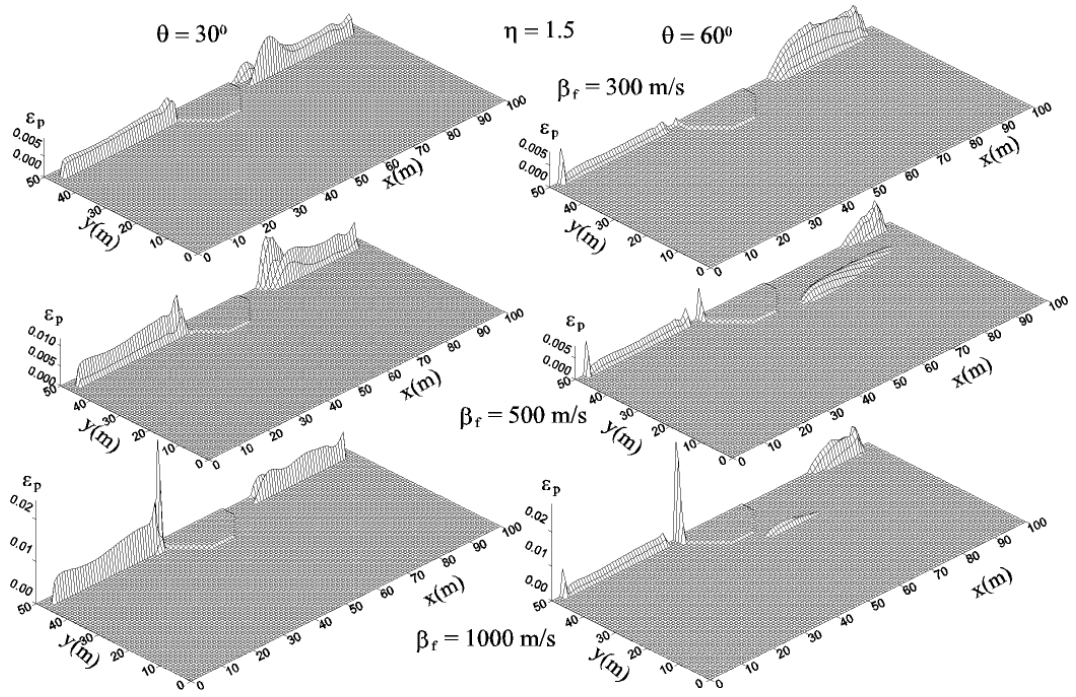

Figure 10d Principal permanent strain in the soil for η = 1.5, two angles of incidence, and three foundation stiffness. C = 1.5

For long pulses, $\eta = 0.1$, it can be seen from figure 9a that for an angle of incidence $\gamma = 30^0$ there is a negligible permanent strain for the stiffest foundation $\beta_f = 1000\ m/s$ only, while for softer foundations the soil remains linear. Also, for intermediate nonlinearity, shown in Fig. 10a, for an angle of incidence $\gamma = 30^0$ it can be seen that in the creation of nonlinear zones the effect of the interaction is negligible compared with the effect of interference of the incoming and the reflected wave from the free surface. For $\gamma = 60^0$, from figures 9a and 10a, it can be concluded that for stiffer foundations the effect of interaction is more dominant than the effect of the interference.

The observations are similar for a five-times-shorter pulse, $\eta = 0.5$ (figures 9b and 10b). For intermediate nonlinearity, C=1.5 (figure 10b) and for the stiffest considered foundation, $\beta_f = 1000\ m/s$, the permanent strain next to the foundation is the largest.

As the pulse becomes shorter, $\eta = 1$, it can be seen that there is creation of nonlinear zones behind the foundation as well. This can be explained by the interference of waves reflected from the free surface and waves diffracted around the foundation. Again, the strain in front of the foundation increases with increasing of the foundation stiffness.

Finally, on figures 9d and 10d the permanent strain distribution is shown for dimensionless frequency of pulse $\eta = 1.5$ in vicinity of which (see figure 7) the hysteretic energies are the highest. It can be seen on figure 10d that for an angle of incidence $\theta = 60^0$ and for stiffer considered foundations,

$\beta_f = 500\text{m/s}, \text{and}\, 1000\text{m/s}$, the zones of permanent strain behind the foundation migrate bellow the free surface. This comes from the interference of the scattered field, which is large for stiff foundation, and the incoming field. This nonlinear zone decreases the energy of the incoming field, which is not strong enough to cause nonlinear zone close to the free surface. For softer foundation, $\beta_f = 300\ \text{m/s}$ the scattered field is not so strong and there is no forming of nonlinear zone below the foundation. In this case the nonlinear zone is formed close to the free surface.

Acknowledgements

This paper is outcome of the research conducted in the Macedonian – Turkish bilateral project "Dynamic analysis of structures with flexible foundation using method of finite differences". This project was financially supported by the Macedonian (MESRM) and Turkish (TUBITAK) Ministries of education and science. On this way we like to express our gratitude to them.

References

[1] H.B. Seed, "Soil problems and soil behaviour", R.L. Wiegel (Ed.). Englewood Cliffs, NJ: Prentice Hall, 1970.

[2] M.D.Trifunac, "Empirical criteria for liquefaction in sands via standard penetration tests and seismic wave energy", Soil Dynamics and Earthquake Eng., 14(6), 419–426, 1995.

[3] M.D. Trifunac, "Interaction of a shear wall with the soil for incident plane SH waves", Bull. Seism. Soc. of America, 62 (1), 63 – 83, 1972.

[4] H.L.Wong, and M.D. Trifunac, "Two-dimensional antiplane, building-soil-building interaction for two or more buildings and for incident plane SH waves", Bull. Seism. Soc. of America, 65(6), 1863–1885, 1975.

[5] A.M. Abdel-Ghaffar, and M.D. Trifunac, "Antiplane dynamic soil-bridge interaction for incident plane SH-waves", Proc. 6th World Conf. on Earthquake Eng., Vol.II, New Delhi, India. 1977.

[6] B.D. Westermo, and H.L. Wong, "On the fundamental differences of three basic soil–structure interaction models", Proc. 6th World Conf. of Eart. Eng., Vol.II, New Delhi, India, 1977.

[7] J.E. Luco, and H.L. Wong, "Dynamic response of rectangular foundations for Rayleigh wave excitation", Proc. 6th World Conf. on Earthq. Eng., Vol.II, New Delhi, India, 1977.

[8] V.W. Lee, "Investigation of three-dimensional soil-structure interaction", Report No. CE 79–11, Dept. of Civil Engineering, Univ. of Southern California, Los Angeles, CA, 1979.

[9] M.I. Todorovska, A. Hayir, and M.D. Trifunac, "Antiplane response of a dike on flexible embedded foundation to incident SH-waves", Soil Dynam. and Earthq. Eng., 21, 593–601, 2001.

[10] A. Hayir, M.I. Todorovska, and M.D. Trifunac, "Antiplane response of a dike with flexible soil-structure interface to incident SH waves", Soil Dynam. and Earthq. Eng., 21, 603–613, 2001.
[11] J. Aviles, M. Suarez, and F.J. Sanchez–Sesma, "Effects of wave passage on the relevant dynamic properties of structures with flexible foundation" Earthq. Eng. and Struct. Dynamics, 31, 139–159, 2002.
[12] V. Gicev, "Investigation of soil-flexible foundation-structure interaction for incident plane SH waves", Ph.D. Dissertation, Dept. of Civil Engineering, Univ. Southern California, Los Angeles, California, 2005.
[13] P. Moczo, "Finite-difference technique for SH-waves in 2-D media using irregular grids—application to the seismic response problem", Geophys. Jour. Int., 99, 321–329, 1989.
[14] J. Zahradnik, P. Moczo, and F. Hron, "Testing four elastic finite-difference schemes for behaviour at discontinuities", Bull. Seism. Soc. of America, 83, 107–129, 1993.
[15] Z. Alterman, and F.C. Caral, "Propagation of elastic waves in layered media by finite difference methods", Bull. Seism. Soc. of Amer., 58 (1), 367–398, 1968.
[16] D.M. Boore, "Finite difference methods for seismic wave propagation in heterogeneous materials", Methods in Comp. Physics 11. New York: Academic Press Inc., 1972.
[17] S.V. Tsynkov, "Numerical solution of problems on unbounded domains: A review", Applied Numerical Mathematics, 27, 465 – 532, 1998.
[18] R.M. Alford, K.R. Kelly, and D.M. Boore, "Accuracy of finite-difference modeling of the acoustic wave equation", Geophysics, 39, 834–842, 1974.
[19] M.A. Dablain, "The application of high-order differencing to the scalar wave equation", Geophysics, 51(1), 54–66, 1986.
[20] D.J. Fah, "A hybrid technique for the estimation of strong ground motion in sedimentary basins", Dissertation, Swiss Federal Institute of Technology, Zurich, Switzerland, 1992.
[21] A.R. Mitchell, "Computational methods in partial differential equations", New York: John Willey & Sons, 1969.
[22] P.D. Lax, and B. Wendroff, "Difference schemes for hyperbolic equations with high order of accuracy", Comm. on Pure and Applied Mathematics, XVII, 381–398, 1964.
[23] K. Aki, and P. Richards, "Quantitative seismology, theory and methods", Publication: W.H. Freeman & Co, 1980.